Structure and Magnetism of VSB-2, -3, and -4 or $Ni_4(O_3P\text{-}(CH_2)\text{-}PO_3)_2\cdot(H_2O)_n$ (n = 3, 2, 0), the First Ferromagnetic Nickel(II) Diphosphonates: Increase of Dimensionality and Multiple Coordination Changes during a Quasi Topotactic Dehydration

Qiuming Gao,[†] Nathalie Guillou,[†] Marc Nogues,[‡] Anthony K. Cheetham,*[,§] and Gérard Férey*[,†]

Institut Lavoisier-Franklin, UMR CNRS 8637 and 8638, Université de Versailles St-Quentin-en-Yvelines, 45 Avenue des Etats-Unis, 78035 Versailles Cedex, France, Chaire Blaise Pascal de l'Ecole Normale Supérieure, 78035 Versailles Cedex, France, and Materials Research Laboratory, University of California, Santa Barbara, 93106 Santa Barbara, California

Received May 28, 1999. Revised Manuscript Received July 19, 1999

$[Ni_4(O_3P\text{-}CH_2\text{-}PO_3)_2\cdot(H_2O)_3$, or VSB-2 was prepared in a pure form under hydrothermal conditions (4−6 days, 453 K, autogenous pressure). It dehydrates in two steps, giving successively the dihydrate VSB-3 at 275 °C and the anhydrous methyl diphosphonate VSB-4 at 350 °C.The structures of the three solids were solved ab initio from X-ray powder data. The three compounds are monoclinic (space group *Cc* for VSB-2 with a = 19.177(3) Å, b = 8.0930(9) Å, c = 9.1824(8) Å, β = 102.387(9)°, and V = 1391.9(2) Å^3, space group *C*2/*c* for VSB-3 and VSB-4 with a = 18.683(4) Å, b = 8.152(2) Å, c = 8.936(2) Å, β = 107.65(1)°, V = 1297.0(3) Å^3; and a = 17.647(2) Å, b = 8.0727(6) Å, c = 8.7741(7) Å, β = 106.339(7)°, V = 1199.5(1) Å^3, respectively). The layered VSB-2 is built from sheets of trimeric edge sharing units of Ni^{2+} octahedra onto which Ni octahedra and diphosphonate groups are grafted. During the first loss (−1 H_2O), the migration of a nickel cation toward a tetrahedral site leads to the connection of the layers and renders the dihydrate VSB-3 three-dimensional. In the totally dehydrated compound VSB-4, stable up to 575 °C, the trimers consist of a central octahedron with two edge-shared square pyramids. The Ni coordinations follow the unique sequence: 4 oct (VSB-2) → 3 oct + tetra (VSB-3) → 1 oct + 2 SQ + tetra (VSB-4) which has drastic effects on the magnetic properties discussed in this paper. Below 4 K, VSB-2 and VSB-4 are indeed canted ferromagnets, whereas VSB-3 is a pure ferromagnet. These open framework phases do not exhibit any porosity.

1. Introduction

The need for new open frameworks with giant pores has become a major thrust in the field of porous solids.[1] The number of the latter, mainly silicates and phosphates, has significantly increased during the last five years and, to date, more than 40 elements have been incorporated as major components into porous compounds.[2] The analysis of the mechanism of formation of these solids under hydrothermal conditions[3] shows, however, that the use of phosphate is a severe limiting factor for obtaining large pores. Moreover, all these systems use organic cations as templating agents and their removal very often leads to the collapse of the inorganic framework. New synthetic approaches giving large pores and avoiding templates are therefore needed.

The pioneering work of Clearfield (see ref 4 and references therein) on the use of phosphonates opened the way. Some research groups, including ours, recently developed new routes for synthesizing microporous solids with accessible porosity. The first strategy was to use diphosphonic acids instead of phosphoric acid. The inorganic part of the acid chelates the cationic species while its organic part, acting as a pillar and a spacer, links the inorganic parts together, frequently leading to pillared three-dimensional structures (see ref 4 and references therein). This method does not need any templating agent, and therefore, the porosity becomes readily accessible.

During the past decade, several one-, two-, or three-dimensional metal phosphonates have been reported (see refs 5−14 and references therein). The contribution of our group concerned first several series (MIL-*n* for

* Authors for correspondence. E-mail: ferey@chimie.uvsq.fr and cheetham@mrl.ucsb.edu
[†] UMR CNRS 8637.
[‡] UMR CNRS 8638.
[§] Chaire Blaise Pascal de l'Ecole Normale Supérieure and University of California.

(1) Férey, G.; Cheetham, A. K. *Science* **1999**, *283*, 213.
(2) Cheetham, A. K.; Férey, G.; Loiseau, T. *Angew. Chem., Int. Ed. Engl.*, in press.
(3) Férey, G. *C. R. Acad. Sci., Sér. C* **1998**, *1*, 1.
(4) Clearfield, A. *Curr. Opin. Solid State Mater. Sci.* **1996**, *1*, 268.
(5) Bonavia, G.; Haushalter, R. C.; Connor, C. J.; Zubieta, J. *Inorg. Chem.* **1996**, *35*, 5603.
(6) Fredoueil, F.; V. Penicaud, V.; Bujoli-doeuff, M.; Bujoli, B. *Inorg. Chem.* **1997**, *36*, 6.

10.1021/cm9910714 CCC: $18.00
Published on Web 09/11/1999

Table 1. Crystallographic Data of the Three Nickel(II) Diphosphonates

compound	VSB-2	VSB-3	VSB-4
formula	$Ni_4(O_3P\text{-}CH_2\text{-}PO_3)_2(H_2O)_3$	$Ni_4(O_3P\text{-}CH_2\text{-}PO_3)_2(H_2O)_2$	$Ni_4(O_3P\text{-}CH_2\text{-}PO_3)_2$
chemical formula weight (g mol^{-1})	632.74	614.73	578.70
calcd density (g cm^{-3})	3.021	3.149	3.206
space group	C c	*C* 2/*c*	*C* 2/*c*
cell parameters	$a = 19.177(3)$ Å	$a = 18.683(4)$ Å	$a = 17.647(2)$ Å
	$b = 8.0930(9)$ Å	$b = 8.152(2)$ Å	$b = 8.0727(6)$ Å
	$c = 9.1824(8)$ Å	$c = 8.936(2)$ Å	$c = 8.7741(7)$ Å
	$\beta = 102.387°$	$\beta = 107.65(1)°$	$\beta = 106.339(7)°$
	$V = 1391.9(2)$ Å^3	$V = 1297.0(3)$ Å^3	$V = 1199.5(1)$ Å^3
figures of merit	$M_{20} = 58$	$M_{20} = 46$	$M_{20} = 86$
	$F_{30} = 119$ (0.0058, 43)	$F_{30} = 84$ (0.0089, 40)	$F_{30} = 127$ (0.0058, 41)
Z	4	4	4
radiation Cu Kα, Å	1.5418	1.5418	1.5418
2θ range, deg	7−100	8−118	8−118
no. of reflections	1429	1850	1733
no. of atoms	25	13	12
no. of structural parameters	76	33	36
R_P	0.077	0.091	0.072
R_{wp}	0.107	0.120	0.092
R_B	0.040	0.107	0.077
R_F	0.034	0.061	0.063

Materials of the Institut Lavoisier) of three-dimensional rare earth diphosphonates;[8] the extension to compounds containing 3d transition metals (M = V, Fe, Ti) led to solids with various dimensionalities: open framework vanadium diphosphonates (MIL-2,[9] -5,[10] and -7[11]), a layered iron diphosphonate MIL-13[12] and a monodimensional titanium diphosphonate MIL-10.[13] Extending the concept, our group has discovered open framework metallic dicarboxylates.[14−18] The use of trimesic acid[19] recently led to the first giant pores in a hybrid organic inorganic solid.

This paper deals with the synthesis, the crystal structures, and the thermal behavior of the first nickel(II) diphosphonates $[Ni_4(O_3P\text{-}CH_2\text{-}PO_3)_2\cdot(H_2O)_n$ (labeled VSB-*m* for Versailles−Santa Barbara (*m* = 2−4)). Their structural study as a function of temperature shows that the quasi topotactic dehydration of the layered trihydrate occurs in two steps. The medium- and high-temperature phases, whose structures were solved ab initio from X-ray powder data, are three-dimensional with slightly open structures.

2. Experimental Section

Synthesis and Chemical Analysis. $Ni_4(O_3P\text{-}CH_2\text{-}PO_3)_2\cdot(H_2O)_3$ was prepared by hydrothermal synthesis (180 °C, 4−6 days, autogenous pressure). In a typical experiment, $NiCl_2\cdot 6H_2O$ (1.75 g) was dissolved in distilled water (5.3 mL); after introduction of tris(2-aminoethyl)amine (TREN, 0.44 mL), pyridine (2.2 mL) was added dropwise before the slow addition of methylenediphosphonic acid (0.65 g). The mixture was stirred until homogeneous, and sealed in Teflon-lined autoclaves (15 mL) with a filling fraction about 70% (volume). After cooling and filtration, the recovered solid (0.6 g; yield 51%) was washed with distilled water and dried at ambient temperature.

Elemental analysis was carried out at the CNRS Center of Analysis (Vernaison). It showed that nickel, phosphorus, and carbon contents were 36.8(1), 19.4(2), and 3.7(2) % (weight), respectively, giving a Ni/P/C ratio of 0.91/1.00/0.49, corresponding to the proposed chemical formula $Ni_4(O_3PCH_2PO_3)_2(H_2O)_3$ (theory 1/1/0.5). No traces of nitrogen were detected in the samples, thus excluding the presence of any organic moiety in the title solid.

The IR spectrum of the compound, carried out on a Nicolet Magna-IR 550 spectrometer using KBr pellets, was assigned as follows: 1091, 1066, 1040, and 1009 cm^{-1} were associated with the asymmetric stretching vibration of PO_4 units, whereas those at 953, 933, 815, 758, and 641 cm^{-1} correspond to symmetric stretching vibration of phosphonate groups; the bands at 589, 564, 482, 451, and 420 cm^{-1} relate to their bending vibration. The strong bands at 3411 and 3309 cm^{-1} correspond to the adsorption of hydroxyl groups, and that at 1373 cm^{-1} to the $-CH_2-$ group.

Thermogravimetric analysis was performed on a TGA 2050 thermogravimetric analyzer under oxygen gas (heating rate 5 °C min^{-1}). The sample is stable until 180 °C without any weight loss, indicating strong bonds for water in the structure. Above this temperature, a quasi one-step 9.7% weight loss occurs, which corresponds to the departure of the water molecules (calcd 8.5%). It is completed at 500 °C. At 950 °C, the resulting solid is the α form of $Ni_2P_2O_7$.

X-ray thermodiffractometry was performed under air in an Anton Paar HTK16 high-temperature device of a Siemens D-5000 diffractometer ($\theta - \theta$ mode) using Co Kα radiation (λ = 1.7903 Å) and equipped with a M Braun linear position sensitive detector (PSD). Patterns were scanned with a resolution of 0.0147° and a divergence slit of 0.1° over an angular range of 5−50° (2θ), up to 1000 °C every 25 °C, with a temperature ramp of 0.1 °C s^{-1}. Evolution of the patterns showed, however, two intermediary phases during the dehydration. The analysis of their structures will be discussed further in this paper.

Structure Determination from X-ray Powder Diffraction. *X-ray Data Analysis and Indexing.* The X-ray powder diffraction data of the three compounds were collected on a Siemens D5000 diffractometer using Cu Kα radiation (λ = 1.5418 Å). To minimize preferred orientation effects, the powder was ground in ethanol with a "McCrone" grinder, dried at 373 K, and then side loaded in the sample holder. The

(7) Lohse, D. L.; Sevov, S. C. *Angew. Chem., Int. Ed. Engl.* **1997**, *36* (15), 1619.
(8) Serpaggi, F.; Férey, G. *J. Mater. Chem.* **1998**, *8*, 2749.
(9) Riou, D.; Roubeau, O.; Férey, G. *Microporous Mesoporous Mater.* **1998**, *23*, 23.
(10) Riou, D.; Serre, C.; Férey, G. *J. Solid State Chem.* **1998**, *141*, 89.
(11) Riou, D.; Férey, G. *J. Mater. Chem.* **1998**, *8*, 2733.
(12) Riou-Cavellec, M.; Serre, C.; Robino J.; Grenèche J. M.; Férey, G. *J. Solid State Chem.*, in press
(13) Ninclaus, C.; Serre, C.; Riou, D.; Férey, G. *C. R. Acad. Sci., Ser. IIc* **1998**, *1*, 551.
(14) Serpaggi, F.; Férey, G. *J. Mater. Chem.* **1998**, *8*, 2737.
(15) Serpaggi, F.; Férey, G. *Microporous Mesoporous Mater.*, in press.
(16) Serpaggi, F.; Férey, G. *Inorg. Chem.*, in press.
(17) Livage, C.; Egger, C.; Noguès, M.; Férey, G. *J. Mater. Chem.* **1998**, *8*, 2743.
(18) Livage, C.; Egger, C.; Férey, G. *Chem. Mater.* **1999**, *11*, 1546.
(19) Chui, S. S. Y.; Lo, S. M., Charmant, J. P. H.; Orpen, A. G.; Williams, I. D. *Science* **1999**, *283*, 1148

Table 2. Comparison of the Coordination Polyhedra in the Three Nickel(II) Diphosphonates[a]

compound			VSB-2	VSB-3	VSB-4
polyhedra					
trimer	central	Ni(2)	NiO_6 octa	NiO_6 octa	NiO_6 octa
	lateral	Ni(1)	$2NiO_5(H_2O)$ octa	$2NiO_5(H_2O)$ octa	$2NiO_5$ sq pyramid
		Ni(3)	$NiO_4(H_2O)_2$ octahedron	NiO_4 tetrahedron	NiO_4 tetrahedron
color			green	blue	brown

[a] For sake of comparison, the labels of the Ni crystallographic sites correspond to the same positions in the three structures.

Table 3. X-ray Powder Diffraction Pattern of VSB-2

hkl	$2\theta_{obs}$ (deg)	$2\theta_{calcd}$ (deg)	d_{obs} (Å)	I_{obs}	*hkl*	$2\theta_{obs}$ (deg)	$2\theta_{calcd}$ (deg)	d_{obs} (Å)	I_{obs}	*hkl*	$2\theta_{obs}$ (deg)	$2\theta_{calcd}$ (deg)	d_{obs} (Å)	I_{obs}
200	9.425	9.436	9.38	100	$\bar{5}12$	29.697	29.702	3.006	8	$\bar{7}12$	36.933	36.912	2.4319	1L
$\bar{1}10$	11.898	11.903	7.43	12	022		29.714			$\bar{2}23$		36.927		
$\bar{1}11$	14.819	14.811	5.97	1	511	29.864	29.841	2.989	1	023	37.375	37.369	2.4041	2
111	16.113	16.113	5.50	2	$\bar{2}22$		29.876			313	37.680	37.685	2.3854	2
$\bar{3}10$	17.928	17.929	4.944	1	402	30.392	30.388	2.939	1L	$\bar{6}22$	38.450	38.454	2.3394	2
400	18.953	18.936	4.679	2	$\bar{6}02$	31.182	31.176	2.866	2	602		38.478		
$\bar{3}11$		18.954			$\bar{1}13$	31.269	31.261	2.858	1	$\bar{1}32$	38.692	38.685	2.3253	3
002	19.783	19.782	4.484	1	421	32.166	32.164	2.781	1	$\bar{4}23$	39.006	39.014	2.3073	1L
$\bar{2}02$	20.008	20.019	4.434	1	222	32.557	32.557	2.748	2	621	39.416	39.392	2.2842	1L
311	21.961	21.937	4.044	2	$\bar{4}22$	32.989	33.004	2.713	1L	004	40.197	40.187	2.2416	1
020		21.948			113	33.208	33.214	2.696	1	$\bar{4}04$	40.680	40.684	2.2161	1L
$\bar{1}12$	22.246	22.249	3.993	1L	$\bar{1}30$	33.531	33.535	2.670	3	$\bar{5}30$	41.215	41.204	2.1886	1L
202	23.741	23.747	3.745	1	$\bar{1}31$	34.727	34.732	2.581	3	$\bar{1}14$	43.099	43.087	2.0972	1L
112	24.021	24.017	3.702	3	710	35.307	35.300	2.540	1	$\bar{6}23$	43.320	43.321	2.0870	1L
$\bar{6}02$	24.331	24.340	3.655	9	$\bar{1}31$		35.337			$\bar{5}32$	43.652	43.642	2.0719	1L
$\bar{2}21$	25.140	25.136	3.539	1	$\bar{6}21$	36.002	35.984	2.4926	2	$\bar{8}21$	43.871	43.901	2.0620	1L
$\bar{5}11$	26.140	26.140	3.406	2	512	36.110	36.099	2.4854	2	513	44.004	44.022	2.0561	1
221	26.715	26.724	3.334	1L	$\bar{3}30$	36.247	36.246	2.4763	2	$\bar{6}22$	44.724	44.735	2.0247	2
$\bar{3}12$	29.041	29.045	3.072	4	$\bar{3}31$	36.797	36.791	2.4406	4	$\bar{3}33$	45.489	45.494	1.9924	1
$\bar{4}21$	29.443	29.451	3.031	4										

Table 4. X-ray Powder Diffraction Pattern of VSB-3

hkl	$2\theta_{obs}$ (deg)	$2\theta_{calcd}$ (deg)	d_{obs} (Å)	I_{obs}	*hkl*	$2\theta_{obs}$ (deg)	$2\theta_{calcd}$ (deg)	d_{obs} (Å)	I_{obs}	*hkl*	$2\theta_{obs}$ (deg)	$2\theta_{calcd}$ (deg)	d_{obs} (Å)	I_{obs}
200	9.936	9.928	8.89	100	$\bar{4}20$	29.696	29.695	3.006	2	$\bar{2}23$	37.360	37.365	2.4051	2
$\bar{1}10$	11.933	11.930	7.41	54	$\bar{2}22$	29.900	29.874	2.986	1L	$\bar{6}20$	37.459	37.458	2.3989	4
$\bar{1}11$	14.808	14.810	5.98	1L	022	30.333	30.332	2.944	8	$\bar{6}22$	38.205	38.253	2.3538	1
111	16.809	16.806	5.27	8	$\bar{6}02$	31.051	31.050	2.878	8	023	38.627	38.621	2.3290	2
$\bar{3}10$	18.490	18.477	4.795	4	312	31.299	31.293	2.856	15	$\bar{1}32$	38.780	38.778	2.3202	1L
$\bar{3}11$	18.860	18.858	4.701	10	$\bar{5}11$	31.949	31.956	2.799	1	512	39.153	39.137	2.9990	2
400	19.942	19.932	4.449	2	$\bar{4}22$	32.729	32.735	2.734	2	422	40.045	40.071	2.2498	1
$\bar{2}02$	20.187	20.191	4.395	1	402	33.220	33.209	2.695	5	$\bar{3}13$	40.659	40.672	2.2172	2
002	20.840	20.846	4.259	4	$\bar{2}22$	33.949	33.988	2.638	1L	$\bar{4}04$	41.057	41.045	2.1966	1
$\bar{1}12$	22.714	22.716	3.912	1	$\bar{1}31$	34.527	34.521	2.596	3	711	41.488	41.486	2.1748	3
$\bar{3}11$	23.381	23.386	3.802	1	$\bar{5}13$	35.664	35.664	2.515	1	$\bar{6}21$		41.500		
402	24.140	24.132	3.684	6	$\bar{1}13$	35.237	35.226	2.544	1	$\bar{3}14$	41.982	41.964	2.1503	1
$\bar{3}12$	24.283	24.292	3.662	13	$\bar{3}30$	36.336	36.333	2.4705	3	004	42.444	42.425	2.1280	1
$\bar{1}12$	25.389	25.385	3.505	3	$\bar{3}31$	36.542	36.538	2.4570	8	$\bar{2}23$		42.452		
$\bar{5}11$	26.384	26.374	3.375	7	$\bar{7}12$	36.895	36.901	2.4343	3	$\bar{6}23$	42.952	42.951	2.1040	1
$\bar{4}21$	29.391	29.391	3.036	17	710	37.010	36.994	2.4270	1	$\bar{6}32$	43.299	43.307	2.0879	1
$\bar{5}12$	29.500	29.478	3.025	2										

powder diffraction patterns were scanned over angular ranges of 7−100° (2θ) for VSB-2, and 8−120° (2θ) for VSB-3 and 4, with a step size of 0.02° (2θ). The counting times were 34 s step^{-1} to 59.78° (2θ) and 68 s step^{-1} from 59.80° (2θ) to the end of the scan for VSB-2; 28 s step^{-1} to 59.98° (2θ) and 56 s step^{-1} in the 60−120° (2θ) range for VSB-3 and -4. This procedure was used to improve the counting statistics of the high-angle region. Full patterns were then scaled to the lower counting time. The contribution of Cu Kα_2 radiation was removed from patterns by means of the software package DIFFRACT-AT and an accurate determination of the peak positions and relative intensities for Cu Kα_1 radiation contribution was carried out. Pattern indexing was performed by means of the computer program DICVOL91[20] from the first 20 lines, with an absolute error in peak positions of 0.03° (2θ). Three monoclinic solutions were found with satisfactory figures of merit. From the complete data sets, reviewed by means of the program NBS*AIDS83,[21] the refined cell parameters given in Tables 1 and 2 were obtained. The powder diffraction data of the three phases are reported in Tables 3−5 for Cu Kα_1 radiation ($\lambda = 1.5406$ Å). Systematic absences were consistent with the two space groups *Cc* and *C*2/*c*.

Structure Solutions and Refinements. Calculations were performed with the EXPO package, integrating EXTRA,[22] a full pattern decomposition program, and SIR*97*.[23] The centric space group *C*2/*c* was chosen first to solve the three structures. Direct Methods and Fourier calculations allowed us to locate all non-hydrogen atoms for the three structures. For VSB-2,

(20) Boultif A.; Louër, D. *J. Appl. Crystallogr.* **1991**, *24*, 987.

(21) Mighell, A. D.; Hubbard, C. R.; Stalik. J. K. NBS*AIDS80: A Fortran Program for Crystallographic Data Evaluation. Nat. Bur. Stand. (U.S.). Technical Note 1141, 1981. (NBS*AIDS83 is an expanded version of NBS*AIDS80.)

(22) Altomare, A.; Burla, M. C.; Giacovazzo, G.; Guagliardi, A.; Moliterni, A. G. G.; Polidori, G. Extra: a Program for extracting Structure-Factor Amplitudes from Powder Diffraction Data. *J. Appl. Crystallogr.* **1995**, *28*, 842.

Table 5. X-ray Powder Diffraction Pattern of VSB-4

hkl	$2\theta_{obs}$ (deg)	$2\theta_{calcd}$ (deg)	d_{obs} (Å)	I_{obs}	*hkl*	$2\theta_{obs}$ (deg)	$2\theta_{calcd}$ (deg)	d_{obs} (Å)	I_{obs}	*hkl*	$2\theta_{obs}$ (deg)	$2\theta_{calcd}$ (deg)	d_{obs} (Å)	I_{obs}
200	10.438	10.439	8.47	100	022	30.657	30.661	2.914	19	$\bar{1}32$	39.246	39.251	2.2937	5
$\bar{1}10$	12.134	12.136	7.29	69	$\bar{5}12$	30.879	30.884	2.893	4	$\bar{6}22$	39.877	39.877	2.2589	1L
$\bar{1}11$	15.058	15.073	5.88	1L	$\bar{3}12$	31.838	31.844	2.808	26	512	40.131	40.133	2.2452	2
111	17.018	17.015	5.21	21	$\bar{6}02$	32.829	32.832	2.726	7	422	40.834	40.841	2.2081	1
$\bar{3}10$	19.174	19.170	4.625	8	$\bar{5}11$	33.080	33.051	2.706	1	$\bar{3}13$	41.256	41.258	2.1865	4
$\bar{3}11$	19.642	19.635	4.516	28	$\bar{3}13$	33.279	33.276	2.690	1	$\bar{4}04$	42.200	42.194	2.1397	2
$\bar{2}02$	20.738	20.736	4.280	5	$\bar{1}30$	33.727	33.698	2.655	8	$\bar{3}14$	42.878	42.870	2.1075	4
400	20.965	20.967	4.234	9	$\bar{4}22$		33.752			530		42.890		
002	21.092	20.086	4.201	2	402	33.967	33.966	2.637	6	$\bar{7}11$	43.155	43.156	2.0946	8
020	21.994	22.004	4.038	2	$\bar{2}22$	34.416	34.420	2.604	1	$\bar{6}23$	44.612	44.617	2.0295	3
$\bar{1}12$	23.060	23.065	3.854	2	$\bar{1}31$	34.917	34.924	2.567	4	$\bar{5}14$	45.259	45.239	2.0020	1L
$\bar{3}12$	25.081	25.084	3.548	18	113	35.617	35.615	2.519	4	$\bar{3}32$		45.266		
$\bar{4}02$	25.275	25.272	3.521	18	$\bar{1}31$	35.849	35.850	2.503	2	$\bar{6}04$	45.941	45.927	1.9738	4
112	25.667	25.667	3.468	6	$\bar{3}30$	36.978	36.978	2.4290	1	$\bar{1}33$		45.944		
202	26.128	26.135	3.408	2	$\bar{3}31$	37.226	37.234	2.4134	12	$\bar{1}14$	46.278	46.284	1.9602	4
$\bar{5}11$	27.748	27.747	3.212	12	$\bar{2}23$	38.004	37.997	2.3658	1	$\bar{2}41$	46.810	46.787	1.9392	1
$\bar{5}10$	28.552	28.558	3.124	1	620	38.900	38.905	2.3133	6	$\bar{8}21$	46.922	46.918	1.9348	1
$\bar{4}21$	30.345	30.352	2.943	24	023	39.071	39.059	2.3036	3					

Table 6. Positional Parameters and Their Standard Deviations for VSB-2[a]

atom	*x*	*y*	*z*
Ni(1_1)	−0.2052(7)	0.1117(9)	−0.434(1)
Ni(1_2)	0.1749(7)	−0.1151(9)	0.457(1)
Ni(2)	0.2322(8)	0.247(1)	0.5000
Ni(3)	0.3496(6)	0.6799(7)	0.247(1)
P(1_1)	0.2878(6)	0.052(1)	0.260(1)
P(1_2)	−0.3153(6)	−0.045(1)	−0.231(1)
P(2_1)	0.3841(6)	0.327(1)	0.400(1)
P(2_2)	−0.4074(6)	−0.333(1)	−0.377(1)
O(1_1)	0.260(2)	−0.166(3)	0.638(3)
O(1_2)	−0.286(2)	0.151(3)	−0.599(2)
O(2_1)	−0.269(1)	−0.068(3)	−0.349(2)
O(2_2)	0.246(1)	0.034(3)	0.372(3)
O(3_1)	0.296(2)	0.111(2)	0.687(3)
O(3_2)	−0.326(2)	−0.132(2)	−0.684(3)
O(4_1)	0.459(1)	0.653(3)	−0.005(3)
O(4_2)	−0.481(1)	−0.622(3)	0.031(2)
O(5_1)	−0.170(1)	−0.138(3)	−0.503(3)
O(5_2)	0.149(1)	0.112(3)	0.536(3)
O(6_1)	0.366(2)	0.412(3)	0.245(2)
O(6_2)	−0.402(1)	−0.433(3)	−0.239(2)
C(1_1)	0.377(1)	0.102(2)	0.368(4)
C(1_2)	−0.404(1)	−0.115(2)	−0.320(4)
O(w1_1)	−0.138(2)	0.225(3)	−0.525(3)
O(w1_2)	0.108(2)	−0.245(3)	0.565(3)
O(w2)	0.458(1)	0.766(2)	0.256(3)

[a] Overall temperature factor is 0.35(6) Å^2. Ni(1_1)and Ni(1_2), independent sites in VSB-2, will be related by a center of symmetry in VSB-3 and -4 and correspond to Ni(1) in the latter structures

Table 7. Positional Parameters and Their Standard Deviations for VSB-3[a]

atom	*x*	*y*	*z*
Ni(1)	0.1861(2)	−0.1044(6)	0.4355(5)
Ni(2)	0.2500	0.2500	0.5000
Ni(3)	0.5000	0.5235(8)	0.2500
P(1)	0.3057(4)	0.0400(9)	0.2583(9)
P(2)	0.4031(3)	0.3176(7)	0.4248(7)
O(1)	0.2770(7)	−0.172(2)	0.626(2)
O(2)	0.2555(8)	0.030(2)	0.351(2)
O(3)	0.3178(8)	0.140(2)	0.689(2)
O(4)	0.4801(5)	0.670(1)	0.046(1)
O(5)	0.1643(6)	0.125(2)	0.534(2)
O(6)	0.4008(7)	0.410(2)	0.271(1)
C(1)	0.3908(9)	0.091(1)	0.393(2)
O(w1)	0.1180(7)	−0.254(2)	0.542(2)

[a] Overall temperature factor is 0.06(2) Å^2.

Table 8. Positional Parameters and Their Standard Deviations for VSB-4[a]

atom	*x*	*y*	*z*
Ni(1)	0.1882(2)	−0.1064(4)	0.4301(3)
Ni(2)	0.2500	0.2500	0.5000
Ni(3)	0.5000	0.5635(6)	0.2500
P(1)	0.3127(3)	0.0372(7)	0.2529(6)
P(2)	0.4138(3)	0.3190(6)	0.4194(7)
O(1)	0.2826(5)	−0.155(1)	0.622(1)
O(2)	0.2576(6)	0.043(1)	0.360(1)
O(3)	0.3174(6)	0.134(1)	0.688(1)
O(4)	0.4935(6)	0.675(1)	0.044(1)
O(5)	0.1590(6)	0.119(1)	0.533(1)
O(6)	0.4113(5)	0.396(1)	0.250(1)
C(1)	0.4076(9)	0.087(2)	0.378(2)

[a] Overall temperature factor is 0.35(6) Å^2.

a third peak was found in a general position with a lower weight than the two first ones. From a study of its environment, we attribute it to a nickel atom (Ni(3) in Tables 6−8) with a half occupancy. The corresponding atomic coordinates were used as starting model in the Rietveld refinement using FULLPROF.[24] A pseudo-Voigt function was selected to describe individual line profiles. To describe the angular dependence of the peak full width at half-maximum, the usual quadratic function in tan θ was used. Unit cells and instrumental parameters were allowed to vary from time to time during the refinement processes. For VSB-3 and -4, one region of the powder pattern was excluded due to the presence of a spurius diffraction line from the dural sample holder. An amorphous part could also be detected for these two samples. Its broad diffraction lines were considered as contributing to the overall background of the diffraction patterns, which was described as a cubic spline function for VSB-3 and -4. The background was refined as a polynomial function for VSB-2. The final Rietveld refinements were carried out in the angular ranges 7−100° (2θ) for VSB-2 and 8−118° (2θ) for VSB-3 and VSB-4. Due to the presence of the Ni(3) atom and its terminal water molecule O(w2) in half occupancy, with this water molecule too close to one of its (∼1.14 Å), we assumed, working on powder diffraction, that the structure of VSB-2 was noncentric to avoid such a disorder. The *x*, *y*, *z* and −*x*, −*y*, −*z* positions were then distinguished and the final refinements attempted in space group *Cc* improved the structure model indicators by about 1%. However, it is clear that this lowering is not sufficient to claim the noncentrosymmetry of VSB-2, owing to the limits of powder diffraction refinements and the lack of statistical tests in such a case. The only merit of space group *Cc* is to suppress statistic disorder. Parts a−c ofFigure

(23) . Altomare, A.; Cascarano, G.; Giacovazzo, C.; Guargliardi, A.; Burla, M. C.; Polidori G.; Camalli., M. *SIR*97: a new tool for crystal structure determination and refinement. *J. Appl. Crystallogr.* **1999**, *32*, 115.

(24) Rodriguez-Carvajal, J. In *Collected Abstracts of Powder Diffraction Meeting*; Toulouse, France, 1990; p 127.

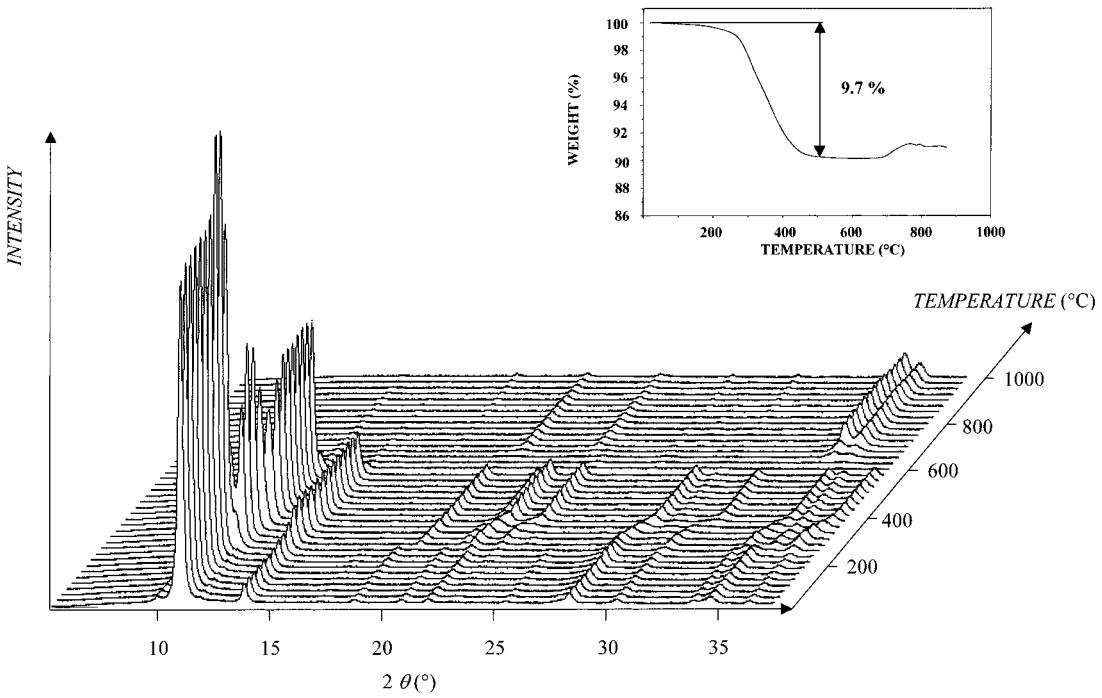

Figure 1. Thermal evolution of the diffractograms during the dehydration of VSB-2 (Co Kα radiation, $\lambda = 1.7903$ Å). Two steps in the dehydration are clearly evidenced while the TGA curve (insert) shows a quasi one-step dehydration.

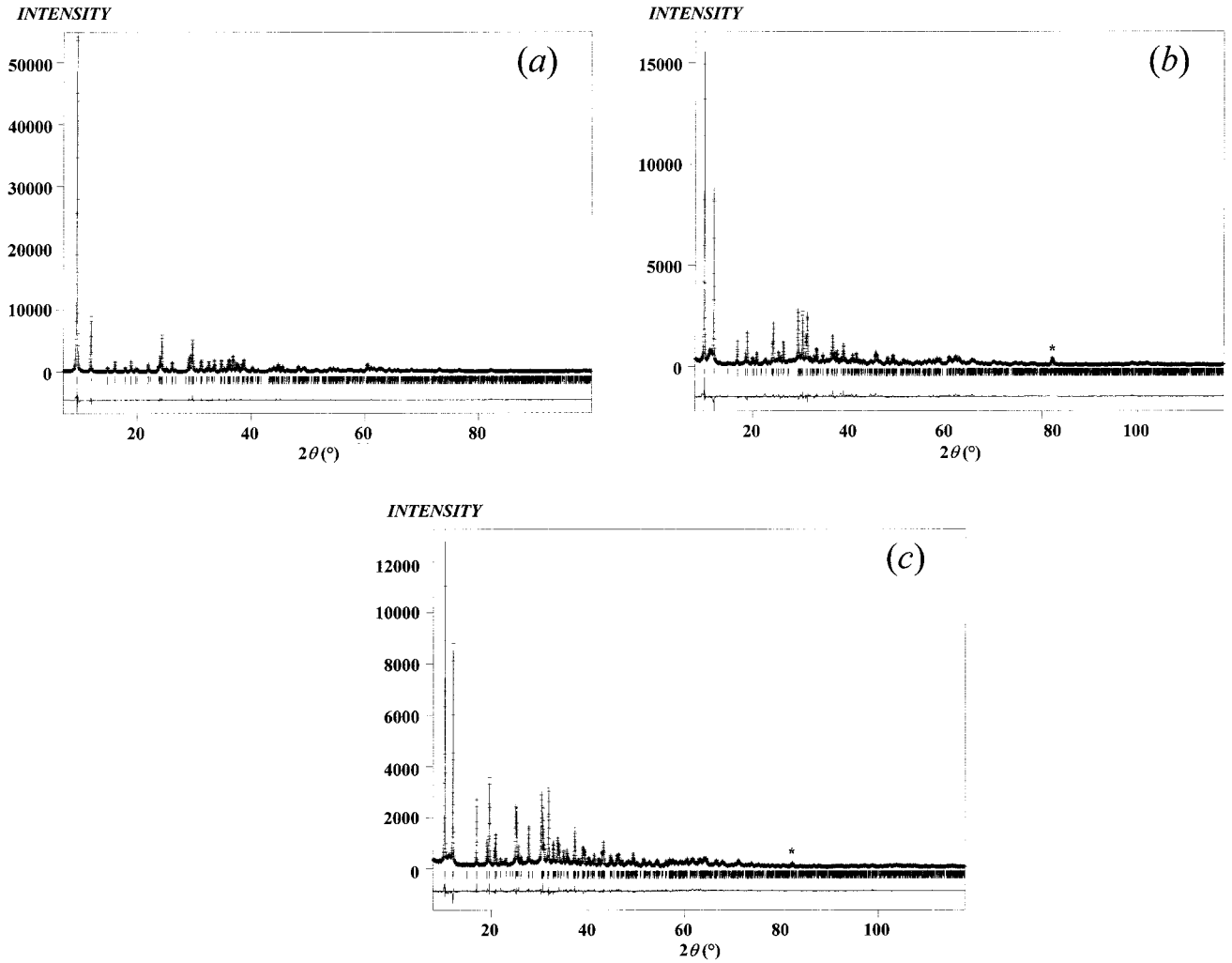

Figure 2. The final Rietveld plots for VSB-2 (a), VSB-3 (b), and VSB-4 (c) (Cu Kα radiation, $\lambda = 1.5418$ Å). Observed data are shown by crosses; the calculated pattern is displayed by the solid line; the lower curve is a plot of the difference, observed minus calculated. (The asterisk (*) indicates the spurius line of the sample holder.)

Table 9. Selected Bond Distances (Å) and Angles (deg) for VSB-2[a]

Within the NiO_6 Octahedra					
$Ni(1_1)-O(1_1)^a$	2.08(3)	$Ni(1_1)-O(6_1)^b$	1.91(3)	$Ni(1_2)-O(2_2)$	2.08(3)
$Ni(1_1)-O(1_2)$	1.95(3)	$Ni(1_1)-O(w1_1)$	1.91(3)	$Ni(1_2)-O(5_2)$	2.08(3)
$Ni(1_1)-O(2_1)$	2.16(3)	$Ni(1_2)-O(1_1)$	2.10(3)	$Ni(1_2)-O(6_2)^d$	2.11(2)
$Ni(1_1)-O(5_1)$	2.26(3)	$Ni(1_2)-O(1_2)^c$	2.14(3)	$Ni(1_2)-O(w1_2)$	2.06(3)
$Ni(2)-O(2_1)^e$	2.05(3)	$Ni(2)-O(5_1)^e$	2.10(3)	$Ni(3)-O(5_1)^f$	2.26(3)
$Ni(2)-O(2_2)$	2.13(3)	$Ni(2)-O(5_2)$	2.02(3)	$Ni(3)-O(6_1)$	2.19(2)
$Ni(2)-O(3_1)$	2.18(3)	$Ni(3)-O(2_1)^f$	2.44(3)	$Ni(3)-O(w1_1)^e$	2.09(3)
$Ni(2)-O(3_2)^e$	2.06(3)	$Ni(3)-O(3_1)^g$	1.99(2)	Ni(3)−O(w2)	2.17(2)
$O(1_1)^a-Ni(1_1)-O(1_2)$	81(2)	$O(2_1)-Ni(1_1)-O(6_1)^b$	89(2)	$O(1_2)^c-Ni(1_2)-O(2_2)$	98(2)
$O(1_1)^a-Ni(1_1)-O(2_1)$	103(2)	$O(2_1)-Ni(1_1)-O(w1_1)$	166(2)	$O(1_2)^c-Ni(1_2)-O(5_2)$	172(2)
$O(1_1)^a-Ni(1_1)-O(5_1)$	177(2)	$O(5_1)-Ni(1_1)-O(6_1)^b$	87(2)	$O(1_2)^c-Ni(1_2)-O(6_2)^d$	100(2)
$O(1_1)^a-Ni(1_1)-O(6_1)^b$	92(2)	$O(5_1)-Ni(1_1)-O(w1_1)$	92(2)	$O(1_2)^c-Ni(1_2)-O(w1_2)$	87(2)
$O(1_1)^a-Ni(1_1)-O(w1_1)$	91(2)	$O(6_1)^b-Ni(1_1)-O(w1_1)$	90(2)	$O(2_2)-Ni(1_2)-O(5_2)$	81(2)
$O(1_2)-Ni(1_1)-O(2_1)$	88(2)	$O(1_1)-Ni(1_2)-O(1_2)^c$	76(2)	$O(2_2)-Ni(1_2)-O(6_2)^d$	88(2)
$O(1_2)-Ni(1_1)-O(5_1)$	99(2)	$O(1_1)-Ni(1_2)-O(2_2)$	87(2)	$O(2_2)-Ni(1_2)-O(w1_2)$	173(2)
$O(1_2)-Ni(1_1)-O(6_1)^b$	172(2)	$O(1_1)-Ni(1_2)-O(5_2)$	96(2)	$O(5_2)-Ni(1_2)-O(6_2)^d$	87(2)
$O(1_2)-Ni(1_1)-O(w1_1)$	94(2)	$O(1_1)-Ni(1_2)-O(6_2)^d$	174(2)	$O(5_2)-Ni(1_2)-O(w1_2)$	94(2)
$O(2_1)-Ni(1_1)-O(5_1)$	74(2)	$O(1_1)-Ni(1_2)-O(w1_2)$	89(2)	$O(6_2)^d-Ni(1_2)-O(w1_2)$	96(2)
$O(2_1)^e-Ni(2)-O(2_2)$	170(2)	$O(3_1)-Ni(2)-O(5_1)^e$	83(2)	$O(3_1)^g-Ni(3)-O(5_1)^f$	83(2)
$O(2_1)^e-Ni(2)-O(3_1)$	86(2)	$O(3_1)-Ni(2)-O(5_2)$	86(2)	$O(3_1)^g-Ni(3)-O(6_1)$	155(2)
$O(2_1)^e-Ni(2)-O(3_2)^e$	97(2)	$O(3_2)^e-Ni(2)-O(5_1)^e$	96(2)	$O(3_1)^g-Ni(3)-O(w1_1)^e$	94(2)
$O(2_1)^e-Ni(2)-O(5_1)^e$	80(2)	$O(3_2)^e-Ni(2)-O(5_2)$	95(2)	$O(3_1)^g-Ni(3)-O(w2)$	100(2)
$O(2_1)^e-Ni(2)-O(5_2)$	99(2)	$O(5_1)^e-Ni(2)-O(5_2)$	169(2)	$O(5_1)^f-Ni(3)-O(6_1)$	81(1)
$O(2_2)-Ni(2)-O(3_1)$	85(2)	$O(2_1)^f-Ni(3)-O(3_1)^g$	80(1)	$O(5_1)^f-Ni(3)-O(w1_1)^e$	177(2)
$O(2_2)-Ni(2)-O(3_2)^e$	92(2)	$O(2_1)^f-Ni(3)-O(5_1)^f$	69(1)	$O(5_1)^f-Ni(3)-O(w2)$	92(2)
$O(2_2)-Ni(2)-O(5_1)^e$	98(2)	$O(2_1)^f-Ni(3)-O(6_1)$	76(1)	$O(6_1)-Ni(3)-O(w1_1)^e$	101(2)
$O(2_2)-Ni(2)-O(5_2)$	81(2)	$O(2_1)^f-Ni(3)-O(w1_1)^e$	109(2)	$O(6_1)-Ni(3)-O(w2)$	100(2)
$O(3_1)-Ni(2)-O(3_2)^e$	177(2)	$O(2_1)^f-Ni(3)-O(w2)$	161(2)	$O(w1_1)^e-Ni(3)-O(w2)$	90(2)
Within Diphosphonate Groups					
$P(1_1)-O(1_1)^h$	1.46(3)	$P(1_1)-C(1_1)$	1.83(3)	$P(1_2)-O(3_2)^i$	1.53(2)
$P(1_1)-O(2_2)$	1.45(3)	$P(1_2)-O(1_2)^i$	1.49(3)	$P(1_2)-C(1_2)$	1.81(3)
$P(1_1)-O(3_1)^h$	1.50(2)	$P(1_2)-O(2_1)$	1.54(3)		
$P(2_1)-O(4_1)^j$	1.52(2)	$P(2_1)-C(1_1)$	1.85(2)	$P(2_2)-O(6_2)$	1.49(2)
$P(2_1)-O(5_1)^e$	1.53(3)	$P(2_2)-O(4_2)^k$	1.53(2)	$P(2_2)-C(1_2)$	1.84(2)
$P(2_1)-O(6_1)$	1.55(2)	$P(2_2)-O(5_2)^l$	1.54(3)		
$O(1_1)^h-P(1_1)-O(2_2)$	116(3)	$O(2_2)-P(1_1)-C(1_1)$	104(2)	$O(1_2)^i-P(1_2)-C(1_2)$	110(3)
$O(1_1)^h-P(1_1)-O(3_1)^h$	105(2)	$O(3_1)^h-P(1_1)-C(1_1)$	105(2)	$O(2_1)-P(1_2)-O(3_2)^i$	116(3)
$O(1_1)^h-P(1_1)-C(1_1)$	115(3)	$O(1_2)^i-P(1_2)-O(2_1)$	109(2)	$O(2_1)-P(1_2)-C(1_2)$	105(2)
$O(2_2)-P(1_1)-O(3_1)^h$	111(3)	$O(1_2)^i-P(1_2)-O(3_2)^i$	111(2)	$O(3_2)^i-P(1_2)-C(1_2)$	105(2)
$O(4_1)^j-P(2_1)-O(5_1)^e$	108(2)	$O(5_1)^e-P(2_1)-C(1_1)$	104(2)	$O(4_2)^k-P(2_2)-C(1_2)$	111(2)
$O(4_1)^j-P(2_1)-O(6_1)$	118(2)	$O(6_1)-P(2_1)-C(1_1)$	107(2)	$O(5_2)^l-P(2_2)-O(6_2)$	111(3)
$O(4_1)^j-P(2_1)-C(1_1)$	103(2)	$O(4_2)^k-P(2_2)-O(5_2)^l$	108(2)	$O(5_2)^l-P(2_2)-C(1_2)$	116(2)
$O(5_1)^e-P(2_1)-O(6_1)$	114(2)	$O(4_2)^k-P(2_2)-O(6_2)$	103(2)	$O(6_2)-P(2_2)-C(1_2)$	107(2)
$P(1_1)-C(1_1)-P(2_1)$	109(1)	$P(1_2)-C(1_2)-P(2_2)$	114(1)		
Most Likely Hydrogen Bonds					
$O(w1_1)\cdots O(4_2)^m$	3.05(4)	$O(w1_2)\cdots O(4_1)^o$	2.89(4)	$O(w2)\cdots O(4_2)^p$	2.80(3)
$O(w1_2)\cdots O(3_2)^n$	2.58(3)	$O(w2)\cdots O(4_1)$	2.57(3)		
$O(3_2)^n\cdots O(w1_2)\cdots O(4_1)^o$	125(2)	$O(4_1)^j\cdots O(w2)\cdots O(4_2)^p$	127(2)		

[a] Symmetry codes: (a) $x - 1/2, y + 1/2, z - 1$; (b) $x - 1/2, 1/2 - y, z - 1/2$; (c) $x + 1/2, y - 1/2, z + 1$; (d) $x + 1/2, -y - 1/2, z + 1/2$; (e) $x + 1/2, y + 1/2, z + 1$; (f) $x + 1/2, 1/2 - y, z + 1/2$; (g) $x, 1 - y, z - 1/2$; (h) $x, -y, z - 1/2$; (i) $x, -y, z + 1/2$; (j) $x, 1 - y, z + 1/2$; (k) $x, -y - 1, z - 1/2$; (l) $x - 1/2, y - 1/2, z - 1$; (m) $x + 1/2, -y - 1/2, z - 1/2$; (n) $x + 1/2, -y - 1/2, z + 3/2$; (o) $x - 1/2, 1/2 - y, z + 1/2$; (p) $x + 1, -y, z + 1/2$.

2 show the final fits obtained between the calculated and observed patterns. They correspond to satisfactory crystal structure model indicators and profile factors (see Table 1). Other details of the refinements are summarized in Table 1. Final atomic parameters are given in Tables 6, 7, and 8, respectively for VSB-2, -3, and -4. Selected bond distances and angles are listed in Tables 9, 10, and 11.

Magnetic Measurements. They were performed using a Squid magnetometer in the temperature range 2−295 K. For all the samples, the magnetization versus temperature M(T) curves were first studied with an applied field of 100 G in order to obtain both the zero-field and field-cooled behavior of the different VSB-m at low fields. Classical M(H) up to 6 T and M(T) measurements in the temperature range 2−295 K then provided the necessary information about magnetization and susceptibility.

3. Results and Discussion

The coupling between TGA and X-ray thermodiffractometry was very fruitful for the completeness of the study. Indeed, despite a quasi one-step decomposition of the original hydrated diphosphonate observed during the TGA experiment (insert of Figure 1), the thermodiffractograms clearly showed (Figure 1) two structural changes before the collapse of the structure at 600 °C, which indicates a rather high stability for such a compound. The residue remains amorphous between

Table 10. Selected Bond Distances (Å) and Angles (deg) for VSB-3[a]

		Within the NiO_x Polyhedra			
Ni(1)−O(1)	2.08(2)	Ni(2)−O(2)	2.25(2)	Ni(3)−O(4)	2.11(1)
Ni(1)−O(1)[a]	2.08(2)	Ni(2)−O(2)[c]	2.25(2)	Ni(3)−O(4)[d]	2.11(1)
Ni(1)−O(2)	2.01(2)	Ni(2)−O(3)	1.99(1)	Ni(3)−O(6)	2.13(1)
Ni(1)−O(5)	2.16(2)	Ni(2)−O(3)[c]	1.99(1)	Ni(3)−O(6)[d]	2.13(1)
Ni(1)−O(6)[b]	2.06(1)	Ni(2)−O(5)	2.00(1)		
Ni(1)−O(w1)	2.18(2)	Ni(2)−O(5)[c]	2.00(1)		
O(1)−Ni(1)−O(1)[a]	74.5(9)	O(2)−Ni(2)−O(2)[c]	180(1)	O(4)−Ni(3)−O(4)[d]	111.0(9)
O(1)−Ni(1)−O(2)	89(1)	O(2)−Ni(2)−O(3)	90(1)	O(4)−Ni(3)−O(6)	113.0(9)
O(1)−Ni(1)−O(5)	96(1)	O(2)−Ni(2)−O(3)[c]	90(1)	O(4)−Ni(3)−O(6)[d]	95.9(8)
O(1)−Ni(1)−O(6)[b]	167(1)	O(2)−Ni(2)−O(5)	82.2(9)	O(4)[d]−Ni(3)−O(6)	95.9(8)
O(1)−Ni(1)−O(w1)	86(1)	O(2)−Ni(2)−O(5)[c]	98(1)	O(4)[d]−Ni(3)−O(6)[d]	113.0(9)
O(1)[a]−Ni(1)−O(2)	94(1)	O(2)[c]−Ni(2)−O(3)	90(1)	O(6)−Ni(3)−O(6)[d]	128(1)
O(1)[a]−Ni(1)−O(5)	170(1)	O(2)[c]−Ni(2)−O(3)[c]	90(1)		
O(1)[a]−Ni(1)−O(6)[b]	93(1)	O(2)[c]−Ni(2)−O(5)	98(1)		
O(1)[a]−Ni(1)−O(w1)	85(1)	O(2)[c]−Ni(2)−O(5)[c]	82.2(9)		
O(2)−Ni(1)−O(5)	84(1)	O(3)−Ni(2)−O(3)[c]	180(1)		
O(2)−Ni(1)−O(6)[b]	93(1)	O(3)−Ni(2)−O(5)	89(1)		
O(2)−Ni(1)−O(w1)	176(1)	O(3)−Ni(2)−O(5)[c]	91(1)		
O(5)−Ni(1)−O(6)[b]	97.0(9)	O(3)[c]−Ni(2)−O(5)	91(1)		
O(5)−Ni(1)−O(w1)	96(1)	O(3)[c]−Ni(2)−O(5)[c]	89(1)		
O(6)[b]−Ni(1)−O(w1)	90.8(9)	O(5)−Ni(2)−O(5)[c]	180(1)		
		Within Diphosphonate Groups			
P(1)−O(1)[e]	1.56(2)	P(1)−C(1)	1.73(2)	P(2)−O(6)	1.56(1)
P(1)−O(2)	1.43(2)	P(2)−O(4)[f]	1.52(1)	P(2)−C(1)	1.87(1)
P(1)−O(3)[e]	1.63(2)	P(2)−O(5)[c]	1.49(0)		
O(1)[e] −P(1)−O(2)	110(2)	O(2)−P(1)−C(1)	104(2)	O(4)[f]−P(2)−C(1)	103(1)
O(1)[e]−P(1)−O(3)[e]	113(2)	O(3)[e]−P(1)−C(1)	106(2)	O(5)[c]−P(2)−O(6)	106(1)
O(1)[e]−P(1)−C(1)	113(2)	O(4)[f] −P(2)−O(5)[c]	119(1)	O(5)[c]−P(2)−C(1)	106(1)
O(2)−P(1)−O(3)[e]	111(2)	O(4)[f]−P(2)−O(6)	112(1)	O(6)−P(2)−C(1)	112(1)
P(1)−C(1)−P(2)	112.9(9)				

[a] Symmetry codes: (a) $^1/_2 - x, -y - ^1/_2, 1 - z$; (b) $^1/_2 - x, y - ^1/_2, ^1/_2 - z$; (c) $^1/_2 - x, ^1/_2 - y, 1 - z$; (d) $1 - x, y, ^1/_2 - z$; (e) $x, -y, z - ^1/_2$; (f) $x, 1 - y, z + ^1/_2$.

Table 11. Selected Bond Distances (Å) and Angles (deg) for VSB-4[a]

		Within the NiO_x Polyhedra:			
Ni(1)−O(1)	2.04(1)	Ni(2)−O(2)	2.10(1)	Ni(3)−O(4)	1.99(1)
Ni(1)−O(1)[a]	2.07(1)	Ni(2)−O(2)[c]	2.10(1)	Ni(3)−O(4)[d]	1.99(1)
Ni(1)−O(2)	1.94(1)	Ni(2)−O(3)	1.97(1)	Ni(3)−O(6)	2.07(1)
Ni(1)−O(5)	2.16(1)	Ni(2)−O(3)[c]	1.97(1)	Ni(3)−O(6)[d]	2.07(1)
Ni(1)−O(6)[b]	2.00(1)	Ni(2)−O(5)	2.01(1)		
		Ni(2)−O(5)[c]	2.01(1)		
O(1)−Ni(1)−O(1)[a]	78.8(7)	O(2)−Ni(2)−O(2)[c]	180.0(9)	O(4)−Ni(3)−O(4)[d]	126.3(9)
O(1)−Ni(1)- O(2)	86.6(8)	O(2)−Ni(2)−O(3)	89.4(7)	O(4)−Ni(3)−O(6)	116.4(8)
O(1)−Ni(1)−O(5)	93.1(7)	O(2)−Ni(2)−O(3)[c]	90.6(7)	O(4)−Ni(3)−O(6)[d]	98.5(8)
O(1)−Ni(1)−O(6)[b]	168.5(9)	O(2)−Ni(2)−O(5)	81.4(7)	O(4)[d]−Ni(3)−O(6)	98.5(8)
O(1)[a]−Ni(1)−O(2)	106.8(8)	O(2)−Ni(2)−O(5)[c]	98.6(8)	O(4)[d]−Ni(3)−O(6)[d]	116.4(8)
O(1)[a]−Ni(1)−O(5)	167.7(9)	O(2)[c]−Ni(2)−O(3)	90.6(7)	O(6)−Ni(3)−O(6)[d]	98.2(7)
O(1)[a]−Ni(1)−O(6)[b]	93.0(7)	O(2)[c]−Ni(2)−O(3)[c]	89.4(7)		
O(2)−Ni(1)−O(5)	81.6(7)	O(2)[c]−Ni(2)−O(5)	98.6(8)		
O(2)−Ni(1)−O(6)[b]	103.7(8)	O(2)[c]−Ni(2)−O(5)[c]	81.4(8)		
O(5)−Ni(1)−O(6)[b]	93.6(7)	O(3)−Ni(2)−O(3)[c]	180.0(9)		
		O(3)−Ni(2)−O(5)	87.1(8)		
		O(3)−Ni(2)−O(5)[c]	92.9(8)		
		O(3)[c]−Ni(2)−O(5)	92.9(8)		
		O(3)[c]−Ni(2)−O(5)[c]	87.1(7)		
		O(5)−Ni(2)−O(5)[c]	180(1)		
		Within Diphosphonate Groups			
P(1)−O(1)[e]	1.47(1)	P(1)−C(1)	1.77(2)	P(2)−O(6)	1.60(1)
P(1)−O(2)	1.53(1)	P(2)−O(4)[f]	1.52(1)	P(2)−C(1)	1.91(2)
P(1)−O(3)[e]	1.51(1)	P(2)−O(5)[c]	1.55(1)		
O(1)[e]−P(1)−O(2)	108(1)	O(2)−P(1)−C(1)	106(1)	O(4)[f]−P(2)−C(1)	99(1)
O(1)[e]−P(1)−O(3)[e]	110(1)	O(3)[e]−P(1)−C(1)	107(1)	O(5)[c]−P(2)−O(6)	109(1)
O(1)[e]−P(1)−C(1)	114(1)	O(4)[f]−P(2)−O(5)[c]	118(1)	O(5)[c]−P(2)−C(1)	111(1)
O(2)−P(1)−O(3)[e]	112(1)	O(4)[f]−P(2)−O(6)	116(1)	O(6)−P(2)−C(1)	102(1)
P(1)−C(1)−P(2)	109.7(9)				

[a] Symmetry codes: (a) $^1/_2 - x, -y - ^1/_2, 1 - z$; (b) $^1/_2 - x, y - ^1/_2, ^1/_2 - z$; (c) $^1/_2 - x, ^1/_2 - y, 1 - z$; (d) $1 - x, y, ^1/_2 - z$; (e) $x, -y, z - ^1/_2$; (f) $x, 1 - y, z + ^1/_2$.

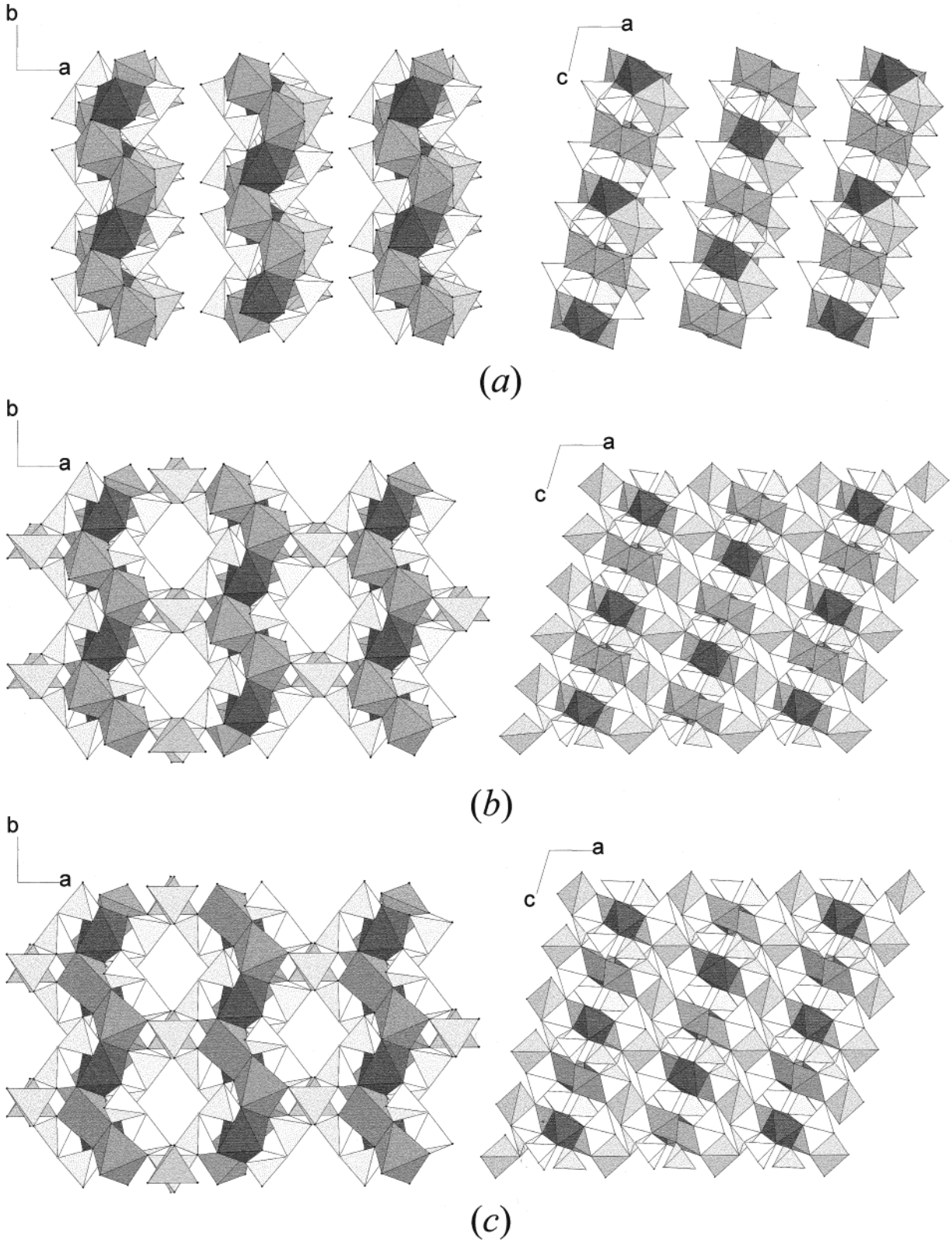

Figure 3. [001] (left) and [010] (right) projections of (a) $Ni_4(O_3P\text{-}CH_2\text{-}PO_3)_2\cdot(H_2O)_3$, (b) $Ni_4(O_3P\text{-}CH_2\text{-}PO_3)_2\cdot(H_2O)_2$, and (c) $Ni_4(O_3P\text{-}CH_2\text{-}PO_3)_2$. The methyldiphosphonate groups are represented as double tetrahedra whose common vertex is the carbon atom of the CH_2 group. The central octahedron Ni(2) appears in dark.

600 and 650 °C. At higher temperatures, $\alpha\text{-}Ni_2P_2O_7$ crystallizes.

The chemical analyses as well as the refinement of the structures show that the transformation corresponds to the following sequence:

$$\underset{\text{VSB-2}}{Ni_4(O_3P\text{-}CH_2\text{-}PO_3)_2\cdot(H_2O)_3} \xrightarrow{275\ ^\circ C} \underset{\text{VSB-3}}{Ni_4(O_3P\text{-}CH_2\text{-}PO_3)_2\cdot(H_2O)_2} \xrightarrow{350\ ^\circ C} \underset{\text{VSB-4}}{Ni_4(O_3P\text{-}CH_2\text{-}PO_3)_2}$$

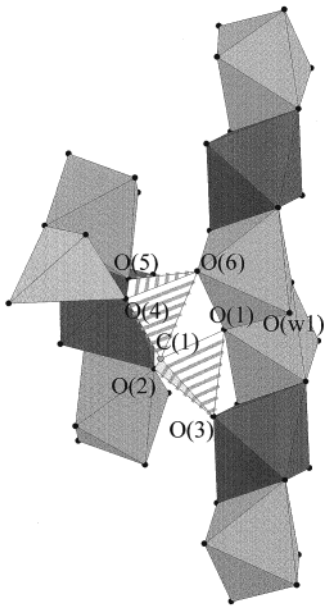

Figure 4. Polyhedral representation of the diphosphonate-grafted trimeric units of Ni(1) and Ni(2) nickel polyhedra common to VSB-3 and VSB-4. The central octahedron Ni(2) appears in dark. The methyl diphosphonate groups are represented by hatched tetrahedra linked by a carbon atom (gray sphere). In VSB-4, The lateral Ni(1) octahedra become square pyramids due to the loss of ligated water molecules (see text).

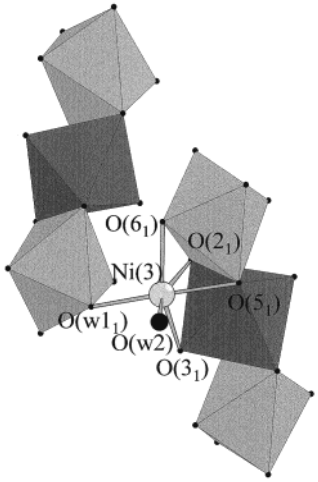

Figure 5. Connection of the octahedron of the nickel Ni(3) (see text) with the central and one lateral octahedra of the trimer in VSB-2.

Figure 3 shows the [001] and [010] projections of the three structures. All of them have monoclinic symmetry with similar cell parameters (see Table 1). The trihydrateVSB-2 assumed to be noncentric (space group *Cc*) is a layered compound, whereas dihydrate VSB-3 (isostructural with the cobalt diphosphonate recently isolated by Sevov et al.[7] and anhydrous VSB-4 are three-dimensional and centric (space group *C* 2/*c*). However, despite strong modifications of some coordination polyhedra during the transformations (Table 2), some common structural features appear from the examination of the three structures and allow a comparative description of the three phases. To render it better, the labeling of the atomic positions is the same in the three structures.

All the structures are built from trimers of edge-sharing Ni(1) and Ni(2) polyhedra, in which the central polyhedron Ni(2) is always an octahedron. These trimers are linked together by one edge to form corrugated chains along the *b* axis. Diphosphonate groups are grafted onto these trimeric units in two ways. Two of the oxygens (O(2) and O(5)) chelate the central octahedron, whereas two others (O(1) and O(6)) are grafted on the two edge-shared octahedra which ensure the linkage between two trimers. In VSB-2 and VSB-3, these two octahedra each bear a water molecule; the latter are in trans position toward the equatorial plane of the bioctahedron.

The position of the nickel atom corresponding to the Ni(3) site explains the difference between VSB-2 and VSB-3. In VSB-2, this nickel is 6-fold coordinated with four oxygens of the trimer, one water molecule of the bioctahedron described above [O(w1$_1$)], and a second water molecule at 2.17(2) Å [O(w2)], which is intrinsic to the structure of VSB-2. The octahedron therefore shares (Figure 5) two consecutive faces with two octahedra of the trimer and one vertex with another trimer of the same layer. The location of the Ni(3) within the layer explains the two-dimensional character of the room temperature form of the diphosphonate.

By heating, O(w2) evolves from the structure, and the position of the Ni(3) becomes unstable within the layer. The cation thus shifts toward the interlayer space in an empty tetrahedral site formed by four oxygens of four different diphosphonate groups, two of them being already shared with nickels of the trimer (Figure 6). This jump implies a slight shift between two layers to

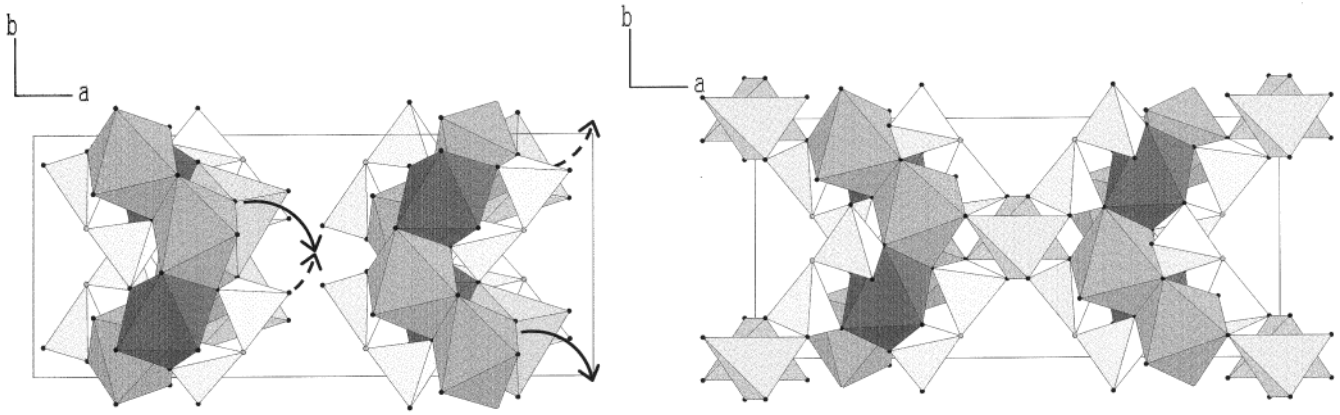

Figure 6. Illustration of the jump of the fourth nickel from an octahedron coordination within the layer to an interlayer tetrahedral site during the transformation VSB-2 → VSB-3.

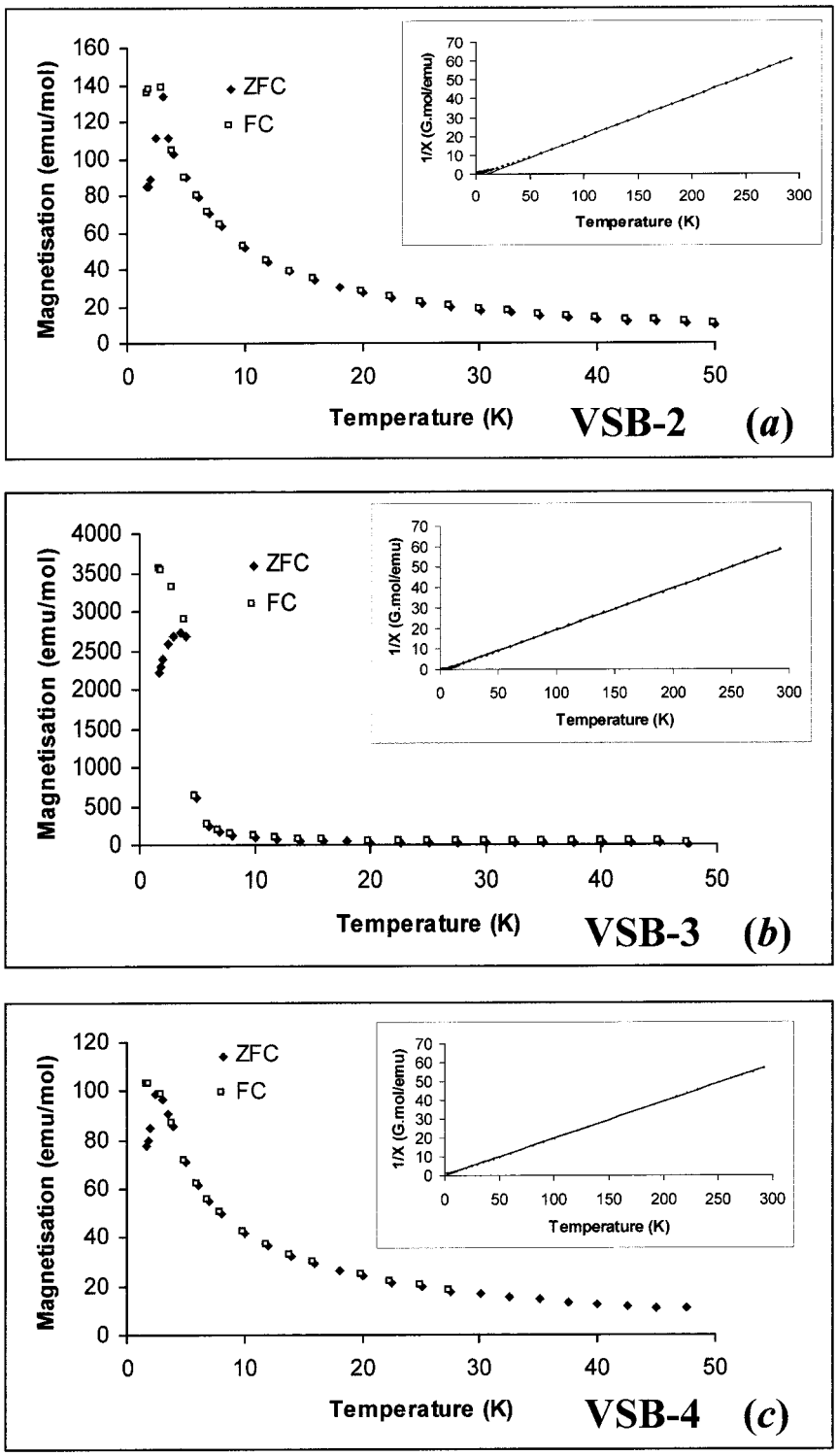

Figure 7. Zero-field cooled (◆) and field cooled (□) M(T) curves under 100 G and, in insert, the inverse susceptibility curves of VSB-2 (a), VSB-3 (b), and VSB-4 (c).

accommodate a real tetrahedral coordination for Ni and explains the small increase of β from 102.4 to 106.7° during the transformation of VSB-2 into VSB-3. Moreover, it ensures a three-dimensional character to VSB-3 in which the nickel subnetwork too becomes three-dimensional.

Further heating above 350 °C transforms VSB-3 into VSB-4. From the structural viewpoint, it corresponds to the loss of the water molecules which belonged to the bioctahedra linking two trimers. Therefore, the trimers of the anhydrous diphosphonate are formed from one central octahedron and two lateral square pyramids and provide a unique example in which nickel(II) is simultaneously 6-, 5-, and 4-fold coordinated. This explains also the different color changes during the dehydration from green to blue and finally to brown. The last stage of dehydration also leads to an important decrease of the *a* parameter (~1 Å) which has two reasons: obviously the loss of water but also a rotation of the connecting NiO_4 tetrahedra around the *y* axis in order

Table 12. Magnetic Characteristics of VSB-2, -3, and -4

compound	VSB-2	VSB-3	VSB-4
μ_{eff} (μB)	2.95(2)	3.14(2)	3.2(2)
θ_p (K)	10.8	4.4	−1.7
T_c magnetization under 100G (emu mol^{-1})	140	2800	90
T_c (K)	3.1(1)	3.8(1)	3.8(2)
magnetization under 6 T at 4K (μB mol^{-1})	4.09 (3)	5.86 (3)	5.01(3)

to have their edges in the [100] and [001] (they deviate from 15°3 toward these directions in VSB-3). This rotation contributes to the decrease of *a*.

The structure of VSB-4 collapses at 600 °C, probably after the reaction of oxygen with the central carbon of the diphosphonate group, which explains the small weight gain observed on the TGA curve. The solid remains amorphous in a short temperature range (600−650 °C) and transforms into α-$Ni_2P_2O_7$ at higher temperatures.

The structural characteristics of the three solids and their evolution have some influence on the different magnetic behaviors. First, as expected from the large number of edge-sharing connections between Ni(II) polyhedra associated with weak 90° superexchange interactions, the magnetic ordering temperatures are very low (Table 12) and with the same order of magnitude regardless of the dimensionality of the VSBs.

The first striking feature concerns the positive (or weakly negative for VSB-4: −1.7 K) values of the paramagnetic Curie temperatures (Curie−Weiss θ) deduced from the inverse susceptibility curves (inserts of Figure 7a−c). This indicates predominant ferromagnetic interactions within the VSBs. Moreover, the characteristic shape of the inverse susceptibility $\chi^{-1}(T)$ curves (inserts of Figure 7a−c) confirms a ferromagnetic behavior for the three phases with Curie constants and effective moments corresponding to Ni^{2+} (Table 12). The zero-field and field-cooled curves under 100 G (Figure 7a−c) provide a good estimation of the magnetic ordering temperatures (Table 12) but evidence the second striking feature concerning these compounds. If the magnetizations of two-dimensional VSB-2 and VSB-4 have similar values at 2 K under 100 G, that of VSB-3 is ∼20 times larger. This indicates a drastic change in the ferromagnetic interactions from two-dimensional VSB-2 to three-dimensional VSB-3 and -4 which is confirmed by the different shapes of the magnetization versus applied field curves at 4 K. The increase of dimensionality could be an explanation of the change between VSB-2 and VSB-3, but cannot be used between VSB-3 and VSB-4. This different behavior is also illustrated by the magnetization versus applied field curves at 4 K (Figure 8). Whereas VSB-2 and 4 exhibit

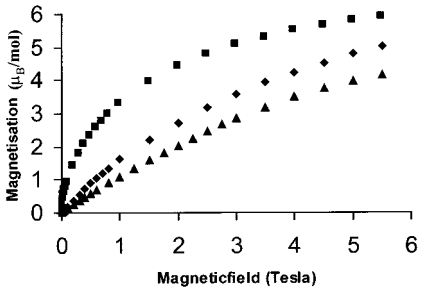

Figure 8. Magnetization (μB mol^{-1}) versus applied field (*T*) of VSB-2 (◆), VSB-3 (■), and VSB-4 (▲).

a slight curvature, VSB-3 is typical of a hard ferromagnet with a net moment of 5.86 μB mol^{-1} under 6T (1.46 μB/Ni). The corresponding values for VSB-2 and -4 are lower, probably indicating a canted ferromagnetic behavior for these two phases. A plausible reason can be found in the coordination changes during the transformations (four octahedra in VSB-2; three octahedra and one tetrahedron in VSB-3; and one octahedron, two square pyramids, and one tetrahedron in VSB-4) and the associated changes in the crystal field degeneracies. That means that no simple model can explain such a complicated behavior. Only the resolution of the magnetic structure by neutron diffraction, which is currently in progress, will give an explanation.

Conclusion

The layered compound $Ni_4(O_3P\text{-}CH_2\text{-}PO_3)_2\cdot(H_2O)_3$, built from sheets of trimeric edge sharing units of Ni^{2+} octahedra on which Ni octahedra and diphosphonate groups are grafted, undergoes two steps of dehydration upon heating. During the first loss (−1 H_2O), the jump of the nickel cation toward a tetrahedral site leads to the connection of the layers and renders the dihydrate three-dimensional. In the totally dehydrated compound, which is stable up to 575 °C, the trimers consist of a central octahedron with two edge-shared square pyramids. The resulting solid does not exhibit any porosity. The evolution of the complex ferromagnetic behavior with structural changes is probably related to the coordination changes, but needs to be quantified by neutron diffraction.

Acknowledgment. Q. Gao gratefully acknowledges CNRS for providing him a postdoctoral position. A. K. Cheetham is very indebted to the Région Ile de France and the Fondation de l'Ecole Normale Supérieure for the Chaire Blaise Pascal he occupied during his two years stay in Versailles.

CM9910714